IEEE Access
Multidisciplinary ⋮ Rapid Review ⋮ Open Access Journal

Received 21 October 2022, accepted 9 November 2022, date of publication 14 November 2022, date of current version 28 November 2022.

Digital Object Identifier 10.1109/ACCESS.2022.3222031

RESEARCH ARTICLE

Controller Design and Disturbance Rejection of Multi-Quadcopters for Cable Suspended Payload Transportation Using Virtual Structure

XIAO HAN[1,2], RYO MIYAZAKI[2], (Member, IEEE), TIANHUA GAO[1], KOHJI TOMITA[2], (Member, IEEE), AND AKIYA KAMIMURA[2], (Member, IEEE)

[1]Graduate School of Science and Technology, University of Tsukuba, Tsukuba 305-8577, Japan
[2]National Institute of Advanced Industrial Science and Technology (AIST), Tsukuba 305-8568, Japan

Corresponding authors: Xiao Han (kan.xiao@aist.go.jp) and Akiya Kamimura (kamimura.a@aist.go.jp)

ABSTRACT Quadcopter is a type of unmanned aerial vehicle (UAV) that offers excellent flight ability albeit with relatively low payload. Despite its widespread use for transportation, improving its robustness against disturbances and carrying capacity has been challenging. Thus, this study proposed a cable suspended multi-UAVs transportation system with a controller and disturbance observer that is highly robust against disturbances. The primary objective of this study is to design a robust controller and disturbance observer by considering the effect of the cable-suspended payload on the UAV as a part of the disturbance. Consequently, reducing the complexity of the problem and allowing a range of algorithms to be used. A controller and disturbance observer are designed based on backstepping control and the extended state of the model, respectively, to control the flight of the multiple UAVs while carrying a cable-suspended payload. Further, to exploit the agility of quadcopters and avoid obstacles, a virtual structure based leader-follower dynamic formation scheme is introduced to change the formation geometry during the flight with cable suspended payload. This scheme does not make any assumption regarding the status of cable tension during the flight and thus no feedback measurement is required from payload. Moreover, the stability analysis of the proposed system is verified theoretically based on Lyapunov stability and through indoor experiments.

INDEX TERMS Cable-suspended payload, disturbance estimation and rejection, leader-follower control, quadcopter, swarm, unmanned aerial vehicles.

I. INTRODUCTION

Drone applications in surveillance, agriculture, payload transportation have witnessed a rapid growth [1], [2]. In particular, the demand for cargo delivery applications is growing at a rapid pace because of its convenience and manpower saving. In addition, the payload transportation via drones requires less infrastructure modification, thereby rendering the system more affordable for commercial users. Certain studies [3] have reported that unmanned aerial vehicles (UAVs) usually have smaller carbon footprint than that of ground-based vehicles. These economic and environmental advantages have resulted in an increased interest in the use of drone systems in logistics.

Certain specially designed drone systems for payload transportation, including drones with a container or grippers, have been proposed [4], [5]. These methods have limited adaptability to the transportation task, considering that factors such as the size and weight of the payload can vary greatly. Simultaneously, using a single drone to transport goods also limits the flight range and carrying capacity, particularly in the case of heavy goods. On certain occasions, large drones are used to address such issues; however, they usually lack agility and are harder to fly in a confined environment, such as in urban areas with many skyscrapers. Moreover, using large drones to deliver small payloads is neither economical nor environmentally friendly. Inspired by UAV SWARM

The associate editor coordinating the review of this manuscript and approving it for publication was Engang Tian.

researchers [6], [7], [8], another method to address the above issues is the use of multiple small drones to transport payloads cooperatively. This approach offers better flexibility because the number of drones can be changed according to the needs of the transportation mission. Further, instead of using specially designed containers or grippers, connecting the drones and cargo through cables provides better adaptability to changes in the shape of the goods. Therefore, this study is mainly focused on the motion control of multiple drones with cable-suspended payloads.

In many situations, position tracking accuracy is critical [9]; however, for package delivery tasks, the safe delivery of payloads is of prime importance. Thus, the robustness of system is more important than the tracking accuracy. Therefore, the designed control system should be sufficiently robust to tolerate unmodeled dynamics and resist disturbances such as wind gust because drones with payload crashing in urban areas can result in unacceptable consequences.

Studies [10], [11], have proposed geometric control of multiple quadcopters with rigid link connected payload, which simplified the control design; however, its usefulness was limited in practical aerial payload transportation situations. In addition, there is no guarantee that the cable remains taut throughout the entire delivery task, particularly in the take-off/landing phases or under disturbances, which should be considered in controller design. In [12], the payload was assumed as a point mass and a hybrid dynamical system was proposed. It addressed the payload sway problem by designing special trajectories of drone. Experimental verifications were presented, but theoretical proof was not provided. In a previous study [13], another controller based on point mass assumption and Lagrangian dynamical model was proposed. It required the cable to stay taut during the flight; however, a method to ensure this assumption was not explained.

In addition to the cable tension assumption, because of the under actuation of a conventional quadcopter, the motion control of quadcopter-payload is complicated [14]. In most studies, the control of quadcopter with payload was considered as the control of double under actuated system. However, certain studies [15], [16] have reported that in contrast to transporting a payload using single drone, because of the mechanical connection between the quadcopter and payload, designing reference trajectories for drones is sufficient to ensure that the payload reached the destination with acceptable accuracy. However, the anti-disturbance approach followed in certain studies [15], [16] does not fully compensate for the effects of disturbances. Thus the anti-disturbance algorithm needs further research. Furthermore, external disturbance such as wind gust is common in the outdoor flight missions and methods to resist such disturbances is an important research topic in the field of UAV control. Several approaches have been proposed for single drone [17], [18], [19], [20], but whether these algorithms can be applied to multi-drone cases still needs to be studied.

TABLE 1. Symbols for calculation.

Symbol	Meaning
$\{\vec{e}_1, \vec{e}_2, \vec{e}_3\}$	Inertial frame
$\{\vec{b}_{i1}, \vec{b}_{i2}, \vec{b}_{i3}\}$	Body fixed frame
$\{\vec{c}_1, \vec{c}_2, \vec{c}_3\}$	Relative formation frame
$x_i(t) \in R^3$	Quadcopter position in inertial frame
$x_{id}(t) \in R^3$	Reference trajectories for ith quadcopter
$x_0(t) \in R^3$	Payload position in inertial frame
$\gamma_i(t) \in R^3$	Relative formation vector
$q_i \in R^3$	A vector directed from the ith quadcopter mass center to the point mass in the inertial frame
m_0	Payload mass
n	Number of quadcopters
m_i	Mass of the ith quadcopter
J_i	Quadcopter inertial moment in body-fixed frame
f_i	Quadcopter thrust in body frame
δ_1, δ_2	Position error and velocity error
$R(\eta_i)$	Rotation matrix
l_i	Length of the ith cable
g	Gravitational acceleration
τ_i	Quadcopter torque control vector in body frame
$\eta_i \triangleq [\phi_i, \theta_i, \psi_i]^T$	Roll-pitch-yaw Euler angle
$\omega_i = [p_i, q_i, r_i]$	Angular velocity in ith quadcopter body-fixed frame

This study proposes a control method for multi-quadcopters with a cable-suspended payload and presents its theoretical stability analysis. Inspired by the research in previous studies [15], [16] and to prioritize safety over accuracy, we propose a method that eliminates the requirement of any measurement or feedback signal from payload. Moreover, in contrast to existing research [10], [11], by treating the cable tension as part of the disturbance, we make no assumptions regarding the cable tension status for controller design. As the proposed payload transportation system is expected to be deployed in a complex environment with many different types of obstacles, a virtual structure based leader–follower dynamic formation approach was considered. We expect the leader drone, with advanced sensors and computers, to detect the obstacles and determine the geometry of the formation in real time, while the follower drones mainly carry the payload and track the formation geometry command given by leader drone. In this paper, the obstacle detection of leader drone is not discussed. In addition, since the external disturbance and unmodeled dynamics of the system are inevitable, disturbance observers are designed to improve the robustness of the control method.

Based on the description above, the contributions of this paper can be summarized as follows:

1) A control scheme, which requires no feedback from payload, is designed for a multi-quadcopter cable-suspended payload transportation system.
2) A linear model-based force disturbance observer and a linear model-based torque disturbance observer are designed to compensate for gravity, cable-tension, wind gust, and unmodeled dynamics.
3) A novel leader-follower dynamic formation method based on virtual-structure is designed for multi-quadcopter payload transportation system to avoid obstacles when flying in constrained environments.

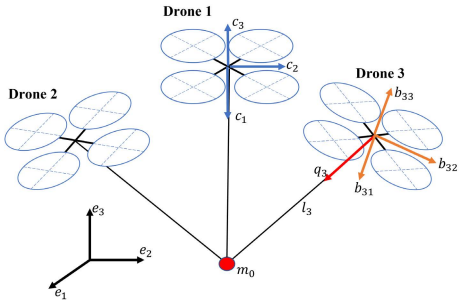

FIGURE 1. Coordinate setting for the transportation of a point mass by multiple quadcopters. The earth, body, and formation frames are depicted in black, orange, and blue, respectively.

4) The proposed control scheme and dynamic formation approach are verified through actual indoor flight experiments.

The remainder of this paper is organized as follows. In Section 2, the dynamics of the multi-quadcopters with cable-suspended payload are described and analyzed. Sections 3 and 4 describe the control method for force control and torque control, and present the disturbance observer design based on the dynamical model of the system. Further, theoretical stable analysis is provided. In Section 5, hardware experiments conducted to verify the control method and disturbance observer are discussed. Section 6 is the conclusion regarding the proposed research on cable-suspended payload transportation system using multi-quadcopters.

II. SYSTEM DYNAMICS

This section introduces the kinematics and dynamics of multi-quadcopter with cable suspended payload transportation system. The key variables are listed in Table 1. As shown in Fig. 1, it is assumed that there are n quadcopters connected to a point mass m_0 via cables of length l_i and negligible mass. An inertial reference frame $\{\vec{e}_1, \vec{e}_2, \vec{e}_3\}$, is fixed on the ground and body-fixed frames $\{\vec{b}_{i1}, \vec{b}_{i2}, \vec{b}_{i3}\}$ for $i \in \{1, 2, 3, \ldots, n\}$, is located at the mass center of ith quadcopter. Whereas, $\{\vec{c}_1, \vec{c}_2, \vec{c}_3\}$ is the relative formation frame and it is designed at the mass center of 1st quadcopter. The relative formation frame is always parallel to inertial reference frame; however, it exhibits transitional motion with respect to 1st quadcopter. Hereinafter, the 1st quadcopter is referred to as the leader quadcopter.

The position of point mass m_0 in the inertial reference frame is denoted by $x_0(t) \in R^3$. Assuming that the cable between ith quadcopter and the point mass is always in taut, the relationship between point mass position and ith quadcopter position is represented by

$$x_i = x_0 - l_i q_i, \tag{1}$$

where $x_i(t) \in R^3$ denotes the position of ith quadcopter in inertial frame and the variable $q_i \in R^3$ represents a vector from ith quadcopter mass center to the point mass in the inertial frame. The above assumption on cable tension is only considered for deriving the relationship between the position of the quadcopter and payload, and is not related to the controller design, which is discussed in the next section.

Under the assumption that the cable mass is negligible, the dynamic equation of multi-quadcopters with cable suspended payload can be expressed as

$$m_i \ddot{x}_i = f_i R(\eta_i)\vec{b}_{i3} - m_i g \vec{e}_{i3} + T_i q_i + D_{i1}(t), \tag{2}$$

$$M(\eta_i)\ddot{\eta}_i + C(\eta_i, \dot{\eta}_i)\dot{\eta}_i = \Psi(\eta_i)^T \tau_i + D_{i2}(t), \tag{3}$$

$$m_0 \ddot{x}_0 = -\sum_{i=1}^{n} T_i q_i - m_0 g \vec{e}_3 + D_3(t). \tag{4}$$

From (2) to (4), $f_i \in [0, f_{max}]$ is the ith quadcopter thrust vector with respect to its body-fixed frame, f_{max} is the maximum thrust, $\tau_i = [\tau_{ix}, \tau_{iy}, \tau_{iz}]^T$ is the torque control vector represented in the ith body-fixed frame for its attitude control, $T_i \geq 0$ is the ith cable tension force magnitude, and $D_{i1}(t), D_{i2}(t), D_3(t)$ are the bounded disturbance acting on the system, which is further discussed in Sections 3 and 4. We use the roll-pitch-yaw Euler angle to represent the quadcopter angular motion. The matrices $M(\eta_i)$ and $C(\eta_i, \dot{\eta}_i)$ in (3) are defined as follows [21].

$$M(\eta_i) = \Psi(\eta_i)^T J_i \Psi(\eta_i), \tag{5}$$

$$C(\eta_i, \dot{\eta}_i) = \Psi(\eta_i)^T (J_i \dot{\Psi}(\eta_i) + (\Psi(\eta_i)\dot{\eta}_i) \times J_i \Psi(\eta_i)), \tag{6}$$

where $\Psi(\eta_i)$ denotes a coordinate transformation matrix that defines the transformation from time derivative of the roll-pitch-yaw Euler angle in the inertial frame to the angular velocity in the ith quadcopter body-fixed frame. Further, $\phi_i, \theta_i \in (-\frac{\pi}{2}, \frac{\pi}{2})$ ensures that $\Psi^{-1}(\eta_i)$ exists.

$$\omega_i = \Psi(\eta_i)\dot{\eta}_i.$$
$$\Psi(\eta_i) = \begin{bmatrix} 1 & 0 & -\sin\theta_i \\ 0 & \cos\phi_i & \cos\theta_i \sin\phi_i \\ 0 & -\sin\phi_i & \cos\theta_i \cos\phi_i \end{bmatrix}. \tag{7}$$

III. FORCE CONTROLLER AND FORCE DISTURBANCE OBSERVER DESIGN

In this section, a virtual-structure based leader-follower dynamic formation scheme is discussed. A force controller and force disturbance observer for the quadcopters are designed. Finally, the stability analysis of the controller and disturbance observer are discussed.

A. REFERENCE TRAJECTORIES

When multi-quadcopters carry a cable-suspended payload to a destination, the design of the reference trajectories for the quadcopters is sufficient for payload transportation, since the payload is physically constrained to the quadcopters via taut cables. The continuously differentiable variable $x_{1d}(t) \in R^3$ denotes the reference trajectories for the leader quadcopter in the inertial frame. $\gamma_i(t) \in R^3$ is the relative formation vector in the relative formation frame. Then, the reference trajectories for the follower quadcopters can be expressed as

$$x_{id}(t) = x_{1d}(t) + \gamma_i(t), \tag{8}$$

where $x_{id}(t)$ denotes the reference trajectories for ith follower quadcopter. Using the above equation, by designing $x_{1d}(t)$ and $\gamma_i(t)$, all the relative virtual structure formation geometric shapes and reference trajectories can be determined. In addition, by changing $\gamma_i(t)$, the relative formation geometric shapes can be flexibly changed during a flight mission to avoid obstacles. To eliminate the possibility of collision between quadcopters, the length of $\gamma_i(t)$ should be set, $\|\gamma_i(t)\| \geq L \cap \|\gamma_i(t) - \gamma_j(t)\| \geq L, i \neq j \in \{2, 3, 4 \ldots, n\}$. L denotes the safety distance between each quadcopter pair.

Another approach for determining reference trajectories for follower quadcopters can be expressed as

$$x_{id}(t) = x_1(t) + \gamma_i(t). \tag{9}$$

In this approach, follower reference trajectories are determined based on the actual position $x_1(t)$ of the leader quadcopter. These two approaches are compared as follows.

Consider n quadcopters. When there is no disturbance in the flight environment, either (8) or (9) can make the follower quadcopters track the leader quadcopter. However, when there is disturbance, such as wind gust, in the flight environment, the actual position of leader quadcopter in the inertial frame will deviate from reference trajectory; that is,

$$x_1(t) = x_{1d}(t) + \Delta x_{dis}(t), \lim_{t\to\infty} \Delta x_{dis}(t) = 0. \tag{10}$$

$\Delta x_{dis}(t)$ denotes the deviation caused by the disturbance. By substituting (10) into (9), it is evident that $\Delta x_{dis}(t)$ travels through the entire formation similar to a wave. However, in (8), $\Delta x_{dis}(t)$ has no influence on other quadcopters as only $x_{1d}(t)$ is passed to the follower quadcopters. Therefore, this study used (8) as the formation algorithm.

B. FORCE CONTROLLER DESIGN

First, the quadcopter dynamic model was simplified by ignoring the attitude dynamics and considering it as a point mass. Then, the quadcopters became fully actuated. By considering gravity and tension of cable in (2) as a part of the disturbance, the translational dynamics of the ith quadcopter can be rewritten as follows:

$$m_i\ddot{x}_i = \mu_i + \widetilde{D}_{i1}(t), \tag{11}$$

where $\mu_i \in R^3$ and $\widetilde{D}_{i1}(t) = -m_i g\vec{e}_{i3} + T_i q_i + D_{i1}(t)$. Therefore, the following control force for each quadcopter could be implemented for position control.

$$\mu_i \triangleq \mu_0 - \widehat{D}_{i1}(t), \tag{12}$$

where $\widehat{D}_{i1}(t)$ is the estimation of $\widetilde{D}_{i1}(t)$ and is discussed later. Here, by ignoring the estimation error between $\widehat{D}_{i1}(t)$ and $\widetilde{D}_{i1}(t)$, the back stepping approach is applied to design the virtual control input μ_0. Substituting (12) into (11) and setting $\delta_1 = x_{id} - x_i$, the following positive-definite Lyapunov function is obtained:

$$m_i\ddot{x}_i = \mu_0, \tag{13}$$

$$V(\delta_1) \triangleq \frac{1}{2}{\delta_1}^2 \geq 0, \tag{14}$$

$$\dot{V}(\delta_1) = \delta_1\dot{\delta}_1. \tag{15}$$

$\dot{V}(\delta_1)$ can be defined as follows:

$$\dot{V}(\delta_1) = \delta_1\dot{\delta}_1 \triangleq -k_1{\delta_1}^2, \tag{16}$$

where $k_1 \in R^{3\times3}$ denotes a positive definite gain matrix. Then, $\dot{V}(\delta_1)$ becomes negative-definite, and x_i is asymptotically stable about the x_{id}. From (16),

$$\dot{\delta}_1 = (\dot{x}_{id} - \dot{x}_i) = -k_1\delta_1.$$

This is rearranged and defined as

$$\dot{x}_{iref} \triangleq \dot{x}_{id} + k_1\delta_1. \tag{17}$$

Let $\delta_2 = \dot{x}_{iref} - \dot{x}_i$. Then, the following positive-definite Lyapunov function can be defined:

$$V(\delta_1, \delta_2) \triangleq \frac{1}{2}{\delta_1}^2 + \frac{1}{2}{\delta_2}^2 \geq 0. \tag{18}$$

$$\dot{V}(\delta_1, \delta_2) = \delta_1\dot{\delta}_1 + \delta_2\dot{\delta}_2. \tag{19}$$

Substituting (17), $\dot{\delta}_1 = (\dot{x}_{id} - \dot{x}_i)$ and $\delta_2 = \dot{x}_{iref} - \dot{x}_i$ in (19) yields

$$V(\delta_1, \delta_2) = \delta_1(\dot{x}_{id} - (\dot{x}_{id} + k_1\delta_1 - \delta_2)) + \delta_2\dot{\delta}_2.$$

Further simplifying the above equation yields

$$\dot{V}(\delta_1, \delta_2) = -k_1{\delta_1}^2 + \delta_2(\dot{\delta}_2 + \delta_1). \tag{20}$$

The first part of the right hand side of the equation is negative definite. If the second part is also negative definite, then $\dot{x}_i$ will be asymptotically stable about the $\dot{x}_{iref}$. It is defined as

$$\delta_2(\dot{\delta}_2 + \delta_1) \triangleq -k_2{\delta_2}^2, \tag{21}$$

$k_2 \in R^{3\times3}$ also denotes a positive definite gain matrix. Simplifying (21), and substituting $\delta_2 = \dot{x}_{iref} - \dot{x}_i$, $\dot{\delta}_2 = \ddot{x}_{iref} - \ddot{x}_i$, and (13) yields

$$\mu_0 = m_i((1 + k_1k_2)(x_{id} - x_i) + (k_1 + k_2)(\dot{x}_{id} - \dot{x}_i) + \ddot{x}_{id}). \tag{22}$$

C. LINEAR MODEL-BASED FORCE DISTURBANCE OBSERVER DESIGN

The disturbance to the quadcopter can be decomposed into force and torque disturbances. Here we design a disturbance observer to compensate the force disturbance. For convenience, $\vec{e}_1, \vec{e}_2, \vec{e}_3$ is defined as the XYZ axis.

Based on the (11), the drone has similar dynamics in the XYZ axis; thus, the X axis was chosen as an example to illustrate the design of the disturbance observer. The position and velocity of the drone in the X axis direction are defined as X_1, X_2 and $X_3 = \widetilde{D}_i$, $X = [X_1, X_2, X_3]^T, X_i \in R^1$. The state equation of the quadcopter is expressed as

$$\dot{X} = AX + Bf_i + E\dot{\widetilde{D}}_i,$$
$$Y = CX,$$

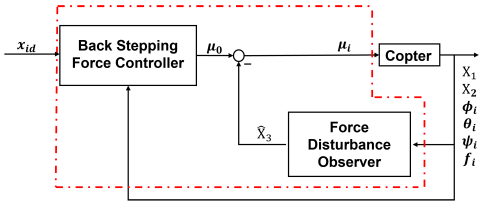

FIGURE 2. Force control block diagram for *i*th quadcopter in the X axis.

TABLE 2. Tunable parameters for force controller and force disturbance observer.

	Tunable Parameters
Back Stepping Force Controller	k_1, k_2
Force Disturbance Observer	W_3

$$A = \begin{bmatrix} 0 & 1 & 0 \\ 0 & 0 & 1 \\ 0 & 0 & 0 \end{bmatrix}, B = \begin{bmatrix} 0 \\ \frac{\xi(\eta_i)}{m_i} \\ 0 \end{bmatrix}, E = \begin{bmatrix} 0 \\ 0 \\ \frac{1}{m_i} \end{bmatrix}, C = \begin{bmatrix} 0 \\ 0 \\ 1 \end{bmatrix}^T. \tag{23}$$

$\xi(\eta_i)$ is a nonlinear function that transforms the thrust from the quadcopter body-fixed frame to the inertial frame. For X axis, $\xi(\eta_i)$ can be written as:

$$\xi(\eta_i) = -\cos\psi_i \sin\theta_i \cos\phi_i - \sin\psi_i \sin\phi_i.$$

For Y and Z axes, $\xi(\eta_i)$ can be obtained from the rotation matrix $R(\eta_i)$. For (23), the following model based disturbance observer is designed:

$$\begin{aligned} \dot{\widehat{X}} &= A\widehat{X} + Bf_i + W(\dot{X}_2 - \frac{\xi(\eta_i)}{m_i} f_i - \widehat{Y}), \\ \widehat{Y} &= C\widehat{X}, \end{aligned} \tag{24}$$

where $\widehat{X} = [\widehat{X}_1, \widehat{X}_2, \widehat{X}_3]^T$, $W = [W_1, W_2, W_3]^T$. $\widehat{X}$ is the estimation of X, and W is the tunable parameter for disturbance observer. $\widehat{X}_i, W_i \in R^1$. As the position X_1 and velocity X_2 can be directly obtained, their estimations $\widehat{X}_2, \widehat{X}_3$ were not used in feedback.

The combination of estimated disturbance $\widehat{X}_3$ in (24) and controller in (22) yields the following final force control equation:

$$\begin{aligned} \mu_i &= m_i((1 + k_1k_2)(x_{id} - x_i) + (k_1 + k_2)(\dot{x}_{id} - \dot{x}_i) \\ &\quad + \ddot{x}_{id}) - \widehat{X}_3, \\ \dot{\widehat{X}}_3 &= W_3(\dot{X}_2 - \frac{\xi(\eta_i)}{m_i} f_i - \widehat{X}_3). \end{aligned} \tag{25}$$

The force control block diagram is shown in Fig. 2, and the tunable parameters are listed in Table. 2.

D. STABILITY ANALYSIS OF FORCE CONTROLLER AND FORCE DISTURBANCE OBSERVER

By considering the fact that the force controller is designed using a back stepping approach and examining (14), (15), (18), and (19), it can be concluded that, if the tunable parameters k_1, k_2 are positive, the force controller satisfies Lyapunov's second method for stability, which ensures the stability of the force controller in (22).

To show the stability of the linear model-based force disturbance observer in (24), subtracting (24) from (23), considering $X_3 = \dot{X}_2 - \frac{\xi(\eta_i)}{m_i} f_i$. Thus, the following equation was obtained:

$$\dot{X} - \dot{\widehat{X}} = (A - WC)(X - \widehat{X}) + E\tilde{D}_i. \tag{26}$$

Eigenvalues of the matrix $(A - WC)$ is $-W_3$, implying that as long as $W_3 > 0$, the linear model-based force disturbance observer is bounded-input bounded-output (BIBO) stable [22]. Furthermore, by providing a large W_3, the convergence speed of the force disturbance observer can be increased, which allows the estimation error between $\widehat{D}_{i1}(t)$ and $\widetilde{D}_{i1}(t)$ to be ignored.

IV. THRUST DIRECTION CONTROLLER AND TORQUE DISTURBANCE OBSERVER

This section introduces the design of thrust direction controller and torque disturbance observer. Thereafter, the stability analyses are provided.

A. THRUST DIRECTION CONTROLLER DESIGN

For (22), the force controller of the quadcopter is designed assuming that the quadcopter is a fully actuated point mass. However, an actual quadcopter can only generate thrust force along the body-fixed frame $\vec{b}_{i3}$; therefore, a thrust direction controller is required to make the thrust direction follow the desired force direction.

Considering (2) and (11), the desired thrust force f_{di} and attitude η_{di} can be calculated as follows:

$$\mu_i = f_{di} R(\eta_{di}) \vec{b}_{i3}. \tag{27}$$

Because (27) is undetermined, the yaw angle is independently controlled. By substituting (5), (6), and (7) into the quadcopter rotation dynamic (3), the following equation in the *i*th quadcopter body-fixed frame is obtained.

$$\begin{aligned} J_i\dot{\omega}_i + \omega_i \times J_i\omega_i &= \tau_i + (\Psi(\eta_i)^T)^{-1} D_{i2}(t), \\ J_i &= \begin{bmatrix} I_{ix} & 0 & 0 \\ 0 & I_{iy} & 0 \\ 0 & 0 & I_{iz} \end{bmatrix}. \end{aligned} \tag{28}$$

By combining (28) and (7), angular acceleration of the Euler angle in the inertial frame can be expressed as follows:

$$\begin{aligned} \ddot{\phi}_i &= \ddot{\psi}_i \sin\theta_i + \dot{\psi}_i\dot{\theta}_i \cos\theta_i \\ &\quad + (\tau_{ix} + q_i r_i (I_{iy} - I_{iz}) + D_{\psi i2})/I_{ix}, \end{aligned} \tag{29}$$

$$\begin{aligned} \ddot{\theta}_i &= \dot{\theta}_i\dot{\phi}_i \tan\phi_i - \ddot{\psi}_i \tan\phi_i \cos\theta_i - \dot{\psi}_i\dot{\phi}_i \cos\theta_i \\ &\quad + \dot{\psi}_i\dot{\phi}_i \tan\phi_i \sin\theta_i \\ &\quad + (\tau_{iy} + p_i r_i (I_{iz} - I_{ix}) + D_{\theta i2})/(I_{iy} \cos\phi_i), \end{aligned} \tag{30}$$

$$\begin{aligned} \ddot{\psi}_i &= \frac{\ddot{\theta}_i \tan\phi_i + \dot{\phi}_i\dot{\theta}_i}{\cos\theta_i} + \dot{\psi}_i\dot{\theta}_i \tan\theta_i + \dot{\psi}_i\dot{\phi}_i \tan\phi_i \\ &\quad + (\tau_{iz} + p_i q_i (I_{ix} - I_{iy}) + D_{\psi i2})/(I_{iz} \cos\phi_i \cos\theta_i), \end{aligned} \tag{31}$$

where $D_{\phi i2}, D_{\theta i2}, D_{\psi i2}$ are portion of $(\Psi(\eta_i)^T)^{-1}D_{i2}(t)$ in each rotation direction. In most cases, angular acceleration $\ddot{\phi}_i, \ddot{\theta}_i, \ddot{\psi}_i$ cannot be measured. Therefore, all terms on the right-hand side of the equation that contain angular acceleration are treated as unmodeled dynamics represented by (29) to (31), and a disturbance observer is designed to estimate them. By considering angular acceleration and other nonlinear functions as parts of the disturbance, (29), (30), and (31) can be rewritten as follows:

$$\ddot{\phi}_i = \Gamma_{ix}(J_i, \eta_i)\tau_{ix} + \widetilde{D}_{\phi i2}, \tag{32}$$
$$\ddot{\theta}_i = \Gamma_{iy}(J_i, \eta_i)\tau_{iy} + \widetilde{D}_{\theta i2}, \tag{33}$$
$$\ddot{\psi}_i = \Gamma_{iz}(J_i, \eta_i)\tau_{iz} + \widetilde{D}_{\psi i2}, \tag{34}$$

where $\Gamma_{ix}, \Gamma_{iy}, \Gamma_{iz}$ is a nonlinear coefficient in each rotation direction. $\widetilde{D}_{\phi i2}, \widetilde{D}_{\theta i2}, \widetilde{D}_{\psi i2}$ are the bounded total disturbances to be compensated by the disturbance observer, where their derivatives are also bounded. It can be seen that roll, pitch, and yaw have similar dynamics from (32) to (34). Here, the roll axis was used to explain the proposed controller and disturbance observer designs.

For roll axis dynamics in (32), $\Gamma_{ix} = 1/I_{ix}$, and τ_{ix} is designed as

$$\begin{aligned}\tau_{ix} &= (\tau_{ix0} - \widehat{D}_{\phi i2})/\,\Gamma_{ix}(J_i, \eta_i) \\ &= (\tau_{ix0} - \widehat{D}_{\phi i2})I_{ix},\end{aligned} \tag{35}$$

where τ_{ix0} is the virtual control input and $\widehat{D}_{\phi i2}$ is the estimation of $\widetilde{D}_{\phi i2}$. τ_{ix0} is calculated via the following equations:

$$\tau_{ix0} = k_3(k_4(\phi_{di} - \phi_i) - \dot{\phi}_i) + k_5\frac{\mathrm{d}(k_4(\phi_{di} - \phi_i) - \dot{\phi}_i)}{\mathrm{d}t}. \tag{36}$$

B. LINEAR MODEL-BASED TORQUE DISTURBANCE OBSERVER DESIGN

Identical to the controller design, the roll axis is used as an example in which the disturbance observer is designed. By choosing $\zeta_1 = \phi_i, \zeta_2 = \dot{\phi}_i, \zeta_3 = \widetilde{D}_{\phi i2}, \zeta = [\zeta_1, \zeta_2, \zeta_3]$, the roll rotation dynamics in (32) is rewritten as state space equation as follows:

$$\dot{\zeta} = \begin{bmatrix}0 & 1 & 0\\ 0 & 0 & 1\\ 0 & 0 & 0\end{bmatrix}\zeta + \begin{bmatrix}0\\ \Gamma_{ix}\\ 0\end{bmatrix}\tau_{ix} + \begin{bmatrix}0\\ 0\\ 1\end{bmatrix}\dot{\widetilde{D}}_{\phi i2}. \tag{37}$$

The state equation in (37) has a structure similar to that of the translational dynamics in (23). Hence, using the angular velocity as the output, a similar disturbance observer is designed as follows:

$$\dot{\widehat{\zeta}} = \begin{bmatrix}0 & 1 & 0\\ 0 & 0 & 1\\ 0 & 0 & 0\end{bmatrix}\widehat{\zeta} + \begin{bmatrix}0\\ \Gamma_{ix}\\ 0\end{bmatrix}\tau_{ix} + \begin{bmatrix}W_4\\ W_5\\ W_6\end{bmatrix}(\zeta_2 - \widehat{\zeta}_2), \tag{38}$$

where $\widehat{\zeta} = [\widehat{\zeta}_1, \widehat{\zeta}_2, \widehat{\zeta}_3]^T$ is the estimation of ζ, $[W_4, W_5, W_6]^T$ is the tunable parameter for the disturbance observer. As the roll angle and roll angular velocity can be obtained from IMU, only the estimated disturbance $\widehat{\zeta}_3$ is used to compensate for the total disturbance.

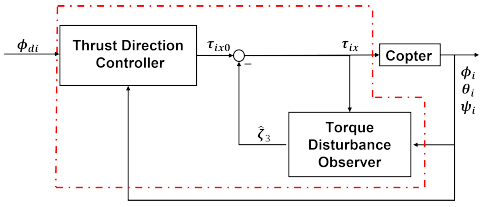

FIGURE 3. Thrust direction control block diagram for the *i*th quadcopter.

TABLE 3. Tunable parameters for thrust direction controller and torque disturbance observer.

	Tunable Parameters
Thrust Direction Controller	k_3, k_4, k_5
Torque Disturbance Observer	W_0

The final torque control signal is calculated using the following equation:

$$\begin{aligned}\tau_{ix} = (&k_3(k_4(\phi_{di} - \phi_i) - \dot{\phi}_i) \\ &+k_5\frac{\mathrm{d}(k_4(\phi_{di} - \phi_i) - \dot{\phi}_i)}{\mathrm{d}t} - \widehat{\zeta}_3)/I_{ix}.\end{aligned} \tag{39}$$

The control block diagram is shown in Fig. 3, and the tunable parameters are listed in Table.3.

C. STABILITY ANALYSIS OF THRUST DIRECTION CONTROLLER AND TORQUE DISTURBANCE OBSERVER

To analyze the stability of thrust direction controller in (36), assuming $\mathcal{L}(\phi_{di}) = \phi_{di}(S)$, $\mathcal{L}(\phi_i) = \phi(S)$, where $\mathcal{L}$ denotes Laplace transform. Combined with (32), (35), and (36) and ignoring the estimation error between $\widetilde{D}_{\phi i2}$ and its estimation $\widehat{D}_{\phi i2}$, we obtain the following transfer function:

$$\frac{\phi(S)}{\phi_{di}(S)} = \frac{(k_4k_5S + k_3k_4)}{((k_5+1)S^2 + (k_3 + k_4k_5)S + k_3k_4)}. \tag{40}$$

If k_3, k_4, and k_5 make the poles of (40) on the left side of the complex plane, the controller in (36) is stable.

As the torque disturbance observer in (38) has a similar structure with the force disturbance observer in (24), their stability analyses are also similar. First, subtracting (38) from (37), we obtain

$$\begin{aligned}\dot{\zeta} - \dot{\widehat{\zeta}} = &\begin{bmatrix}0 & 1 & 0\\ 0 & 0 & 1\\ 0 & 0 & 0\end{bmatrix}(\zeta - \widehat{\zeta}) - \begin{bmatrix}W_4\\ W_5\\ W_6\end{bmatrix}(\zeta_2 - \widehat{\zeta}_2) \\ &+ \begin{bmatrix}0\\ 0\\ 1\end{bmatrix}\dot{\widetilde{D}}_{\phi i2}.\end{aligned}$$

Simplification of this equation yields

$$\dot{\zeta} - \dot{\widehat{\zeta}} = A_2(\zeta - \widehat{\zeta}) + \begin{bmatrix}0\\ 0\\ 1\end{bmatrix}\dot{\widetilde{D}}_{\phi i2}.$$
$$A_2 = \begin{bmatrix}0 & 1 - W_4 & 0\\ 0 & -W_5 & 1\\ 0 & -W_6 & 0\end{bmatrix}. \tag{41}$$

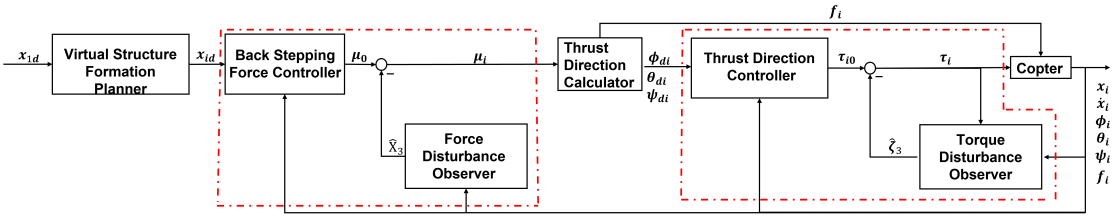

FIGURE 4. Complete system control block diagram. The x_{1d} is predefined. x_{id} is automatically calculated (formation vector γ is given by user) and sent to each quadcopter. Desired yaw angle ψ_{di} is set to 0. In the feedback data, roll and pitch angle are obtained from IMU of each quadcopter, whereas the yaw angle and position are obtained from the motion capture system.

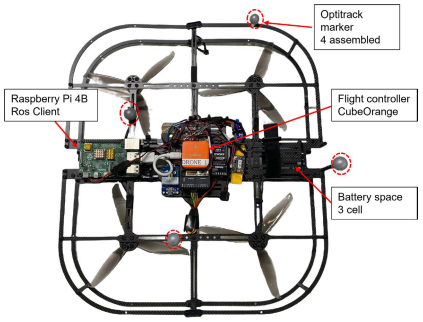

FIGURE 5. Quadcopter setup for the experiment. Raspberry Pi 4B works as the ROS client to communicate with ROS master. Raspberry Pi 4B receives target position x_{id} from ROS master and actual position x_i from motion capture system, which are then sent to the flight controller.

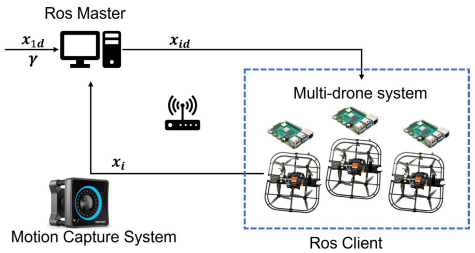

FIGURE 6. System setup for the experiment. Target position for leader quadcopter and formation vector γ are predefined by user. Target positions of follower quadcopters are calculated by ROS master then sent to each drone via WiFi.

By computing the characteristic polynomials of the matrix A_2, its eigenvalues are determined to be $\frac{-W_5 \pm \sqrt{W_5{}^2 - 4W_6}}{2}$. This implies that, if $W_5 > 0$ and $W_6 > 0$ are satisfied, (41) is guaranteed to be BIBO stable. To simplify the parameter tuning, the eigenvalues of the matrix are set to $-W_0$, which yield the parameters $W_5 = 2W_0$, $W_6 = W_0{}^2$.

The control block diagram of the complete system is shown in Fig. 4, where the force controller and force disturbance observer are calculated using (22) and (24). Formation planner is calculated using (8). Thrust direction is calculated using (27) and yaw is manually set to 0. Thrust direction controller and torque disturbance observer are calculated using (36) and (38). The corresponding adjustable parameters are listed in Tables. 2 and 3, respectively.

V. EXPERIMENTS AND RESULTS

This section presents several experiments to confirm the proposed control approach followed by the results obtained.

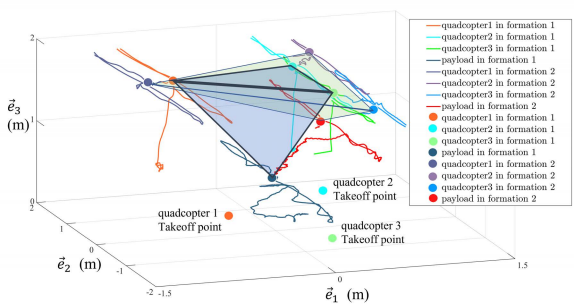

FIGURE 7. Trajectory of three quadcopters with cable-suspended payload in experiment 1. The take-off and landing phases have been omitted to make the diagram clearer. The two tetrahedrons in the figure correspond to the two formations. The change in the position of the payload during the two formations demonstrates that the position of the payload can be effectively controlled by dynamic formation.

A. EXPERIMENT SETUP

To validate the proposed approach, experiments were conducted using three quadcopters with cable-suspended payloads. The quadcopters were square shaped measuring 40 cm in length and weighing 800g including the batteries. The length of the cable was 1.2 m, and its mass was negligible. Further, the payload weight was 300g, and its geometry was ignored and thus treated as a point mass.

The flight control program of the UAV was written based on the ardupilot open source program. The control-related programs were replaced by the algorithms presented in Sections 3 and 4. The force and thrust direction control loops were run at 400 and 200 Hz, respectively. In the execution of each control loop, the controller functions are called first, and then the disturbance observer update functions are called.

The ROS system was installed on Raspberry Pi and was used to obtain the target position of each quadcopter. The formation vector γ_i was provided manually in the experiment. Adaptive determination of the formation vector γ_i will be discussed in a future study on multi-quadcopters formations. Further, a motion capture system was used for feedback and data recording in experiments. Four sets of experiments were conducted.

B. EXPERIMENT 1: DYNAMIC FORMATION AND TRANSLATIONAL MOVEMENT

In the first experiment, three quadcopters were used to deliver the payload without wind disturbance. The geometry of the

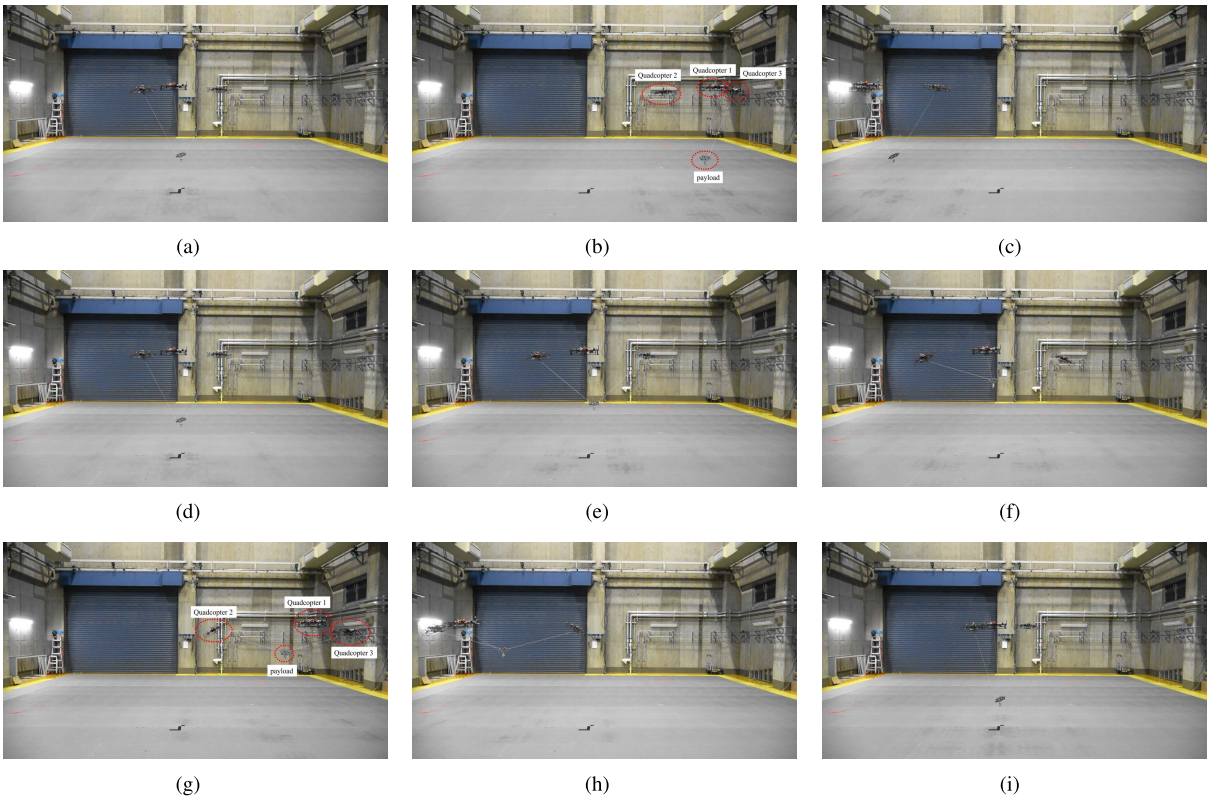

FIGURE 8. Dynamic formation of three quadcopters with cable-suspended payload. (a)–(c) show the movement of three quadcopters under first formation structure, where $\gamma_2 = [1 \quad 0.6 \quad 0]^T$, $\gamma_3 = [1 \quad -0.6 \quad 0]^T$, (d)–(f) show the dynamic formation reconfiguration with a cable-suspended payload. (g)–(i) show the movement of three quadcopters under a second formation structure, where $\gamma_2 = [1.65 \quad 0.95 \quad 0]^T$, $\gamma_3 = [1.65 \quad -0.95 \quad 0]^T$, that then changes back to the first formation structure.

quadcopter formations changed during the delivery process. For the first formation geometry, relative formation vectors were set to $\gamma_2 = [1\ 0.6\ 0]^T$, $\gamma_3 = [1\ -0.6\ 0]^T$. Whereas, for second formation geometry, relative formation vectors were set to $\gamma_2 = [1.65\ 0.95\ 0]^T$, $\gamma_3 = [1.65\ -0.95\ 0]^T$.

Fig. 7 shows the trajectory of three quadcopters and payload in experiment. After take-off, the quadcopters move along the $\vec{e}_2$ of the ground coordinate system in formation 1 with the cable-suspended payload. Here, the target position of the leader quadcopter changes from $[-0.75\ -2\ 1.8]^T$ to $[-0.75\ 2\ 1.8]^T$. The follower quadcopters 2 and 3 calculated the target positions based on the relative formation vectors. After returning to the vicinity of the origin, the geometric transformation of the formation was performed. It was observed that with the change in the geometry of the formation, the altitude of the payload also changed from low to high. This change was reflected in the relative position of the red dot, which shifted from a lower altitude to a higher one, as shown in Fig. 7. After completing the formation transformation, three quadcopters again moved along $\vec{e}_2$, where the target positions of leader quadcopter were changed from $[-1.15\ -2\ 1.8]^T$ to $[-1.15\ 2\ 1.8]^T$. The follower quadcopters 2 and 3 also moved to the target positions based on the new relative formation vectors.

Fig. 8 shows the snap shot of experiment 1, where (a)-(c) show the movement of three quadcopters and cable-suspended payload in formation 1; (d)–(f) is the process of geometric changes in formations; (f)-(h) show the movement of three quadcopters in formation 2; and (i) shows the three quadcopters returning to origin at the end of experiment. Fig. 9 shows the positions of each quadcopter in experiment 1. Here, (a)–(c) indicate the target altitude and actual altitude of each quadcopter. Compared to [16], it is evident that there is no steady-state errors at altitude, implying that the proposed force disturbance observer in control scheme fully compensated for gravity. Further, (d)–(f) show the target position and actual position in $\vec{e}_1$. The tracking errors were always less than 10 cm and no steady-state errors remained. Same results were observed from (g)-(i), which are the target position and actual position in $\vec{e}_2$. There was a lag in position tracking between 80 s and 100 s owing to mutual pulling of quadcopters 2 and 3. This indicates the need for integrated control of output forces of drones.

Based on the flight experiments, the parameter selection rules can be further described as follows: W_3, W_0 must be positive and large enough to make the estimation error negligible but must be set so that the noise signal does not cause oscillations. For our drones, we selected W_0 as 50, W_3 as 1. k_1, k_2, k_3, k_4 must be positive and large enough to make the convergence speed of force controller and thrust direction controller fast, but not too large that they cause an overshoot, and k_5 can be carefully adjusted to suppress the overshoot in

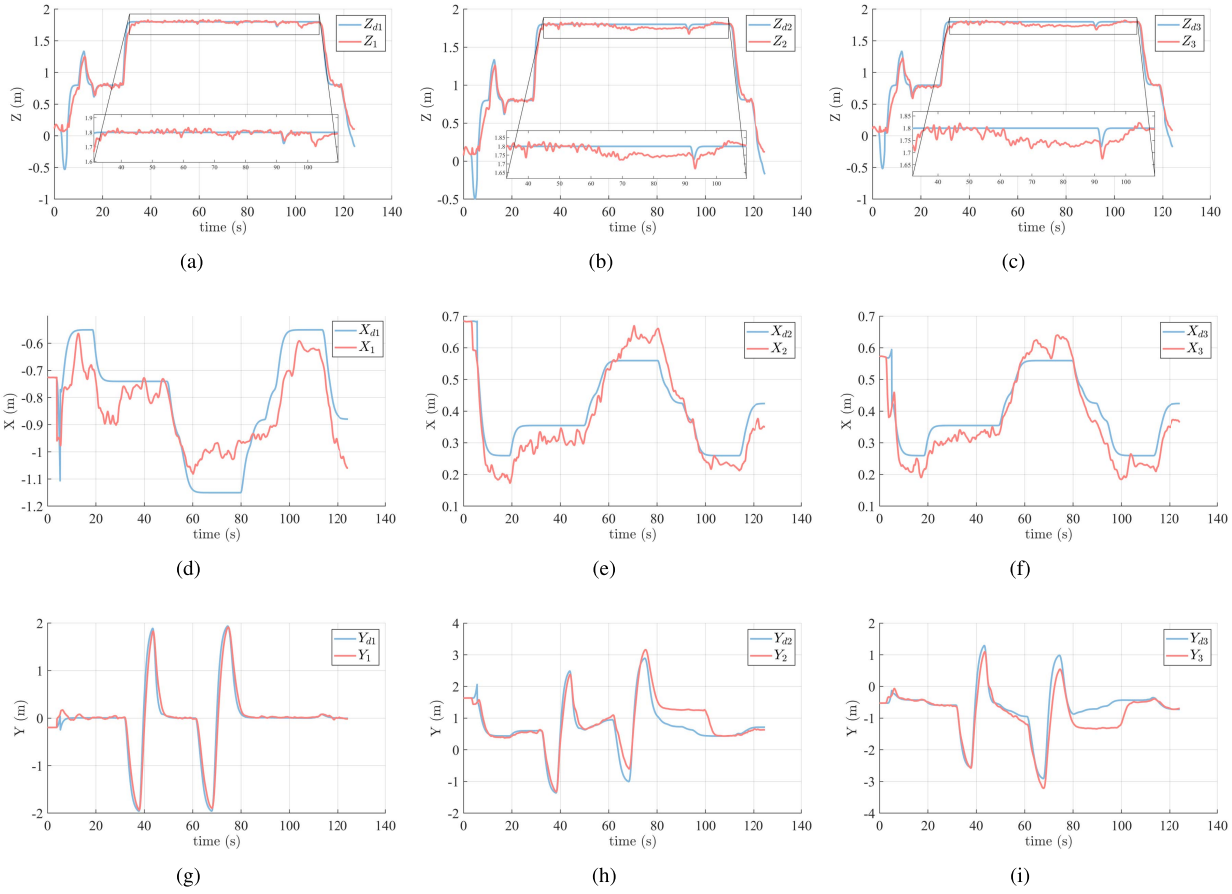

FIGURE 9. Resulting logs of each quadcopter in the first experiment. Blue lines are the target positions and red lines are the actual positions.

thrust direction tracking. For our drones, we selected k_1, k_2 as identity matrix, k_3 as 9, k_4 as 0.135 and k_5 as 0.004.

C. EXPERIMENT 2: DYNAMIC FORMATION AND TRANSLATIONAL MOVEMENT UNDER WIND DISTURBANCE

In this experiment, three quadcopters with cable-suspended payload tracked the target position under wind disturbance. The formation was also changed in this experiment, as in the first experiment.

Fig. 10 (a) shows a snapshot of the experiment. The left side of the image shows the blower that was used to generate wind turbulence, which generated wind speeds of 3–7 m/s measured at the test site. The right side of the image shows the three quadcopters with the cable-suspended payload.

In the Fig. 10 (b), trajectory of the three quadcopters and payload are shown. The take-off and landing trajectories were omitted to make the results clearer. The blue area shows the area affected by wind disturbance.On examining the trajectory in Fig. 10 (b), it is confirmed that the three quadcopters and payload first traveled through the wind disturbance area along the $\vec{e}_1, \vec{e}_2$ in formation 1, where $\gamma_2 = [1\ 0.6\ 0]^T$, $\gamma_3 = [1\ -0.6\ 0]^T$. Then, the relative formation vectors changed to $\gamma_2 = [1.65\ 0.95\ 0]^T$, $\gamma_3 = [1.65\ -0.95\ 0]^T$ in order to transform to formation 2. The three quadcopter and payload again traveled through the wind disturbance area along the $\vec{e}_1, \vec{e}_2$.

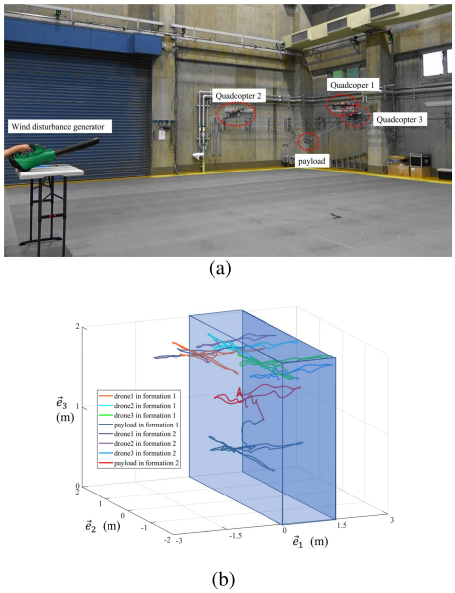

FIGURE 10. Experiment 2 setup with wind disturbance generator. (a) shows the snap shot of experiment. (b) shows the trajectory of three quadcopters and payload in experiment 2, blue area is the wind area and maximum wind speed is 20 km/h.

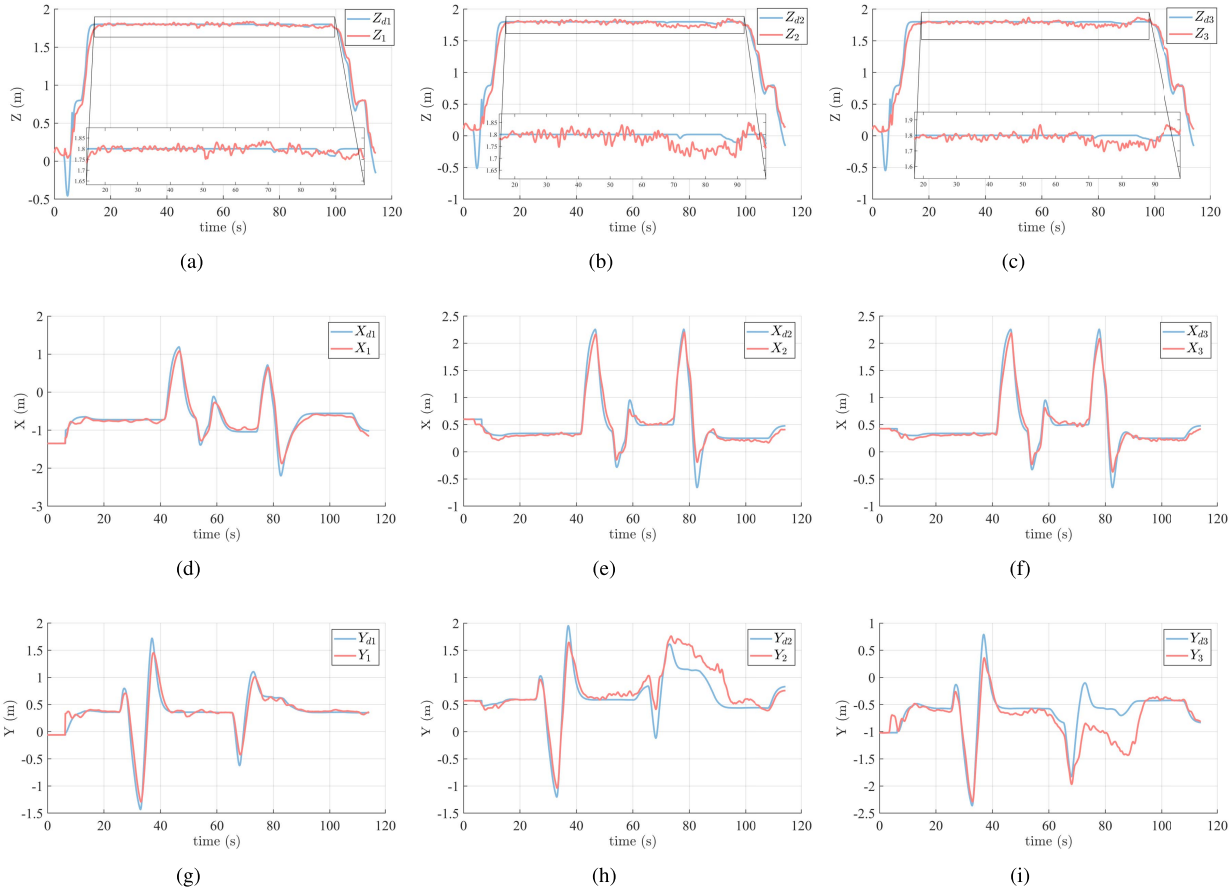

FIGURE 11. Logs of each quadcopter in the second experiment. Blue lines represent the target positions and red lines denote the actual positions.

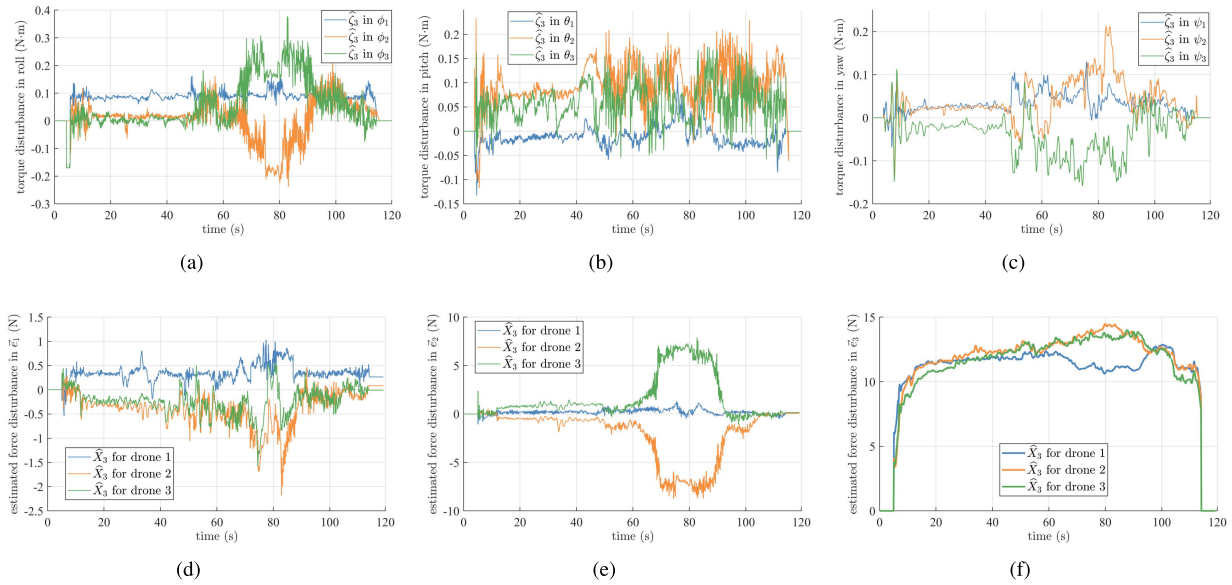

FIGURE 12. Estimated torque disturbance in roll-pitch-yaw and estimated force disturbance in the inertial frame for three quadcopters with a cable-suspended payload under wind disturbance.

Fig. 11 shows the target position and actual position for each quadcopter in $\vec{e}_1, \vec{e}_2, \vec{e}_3$ under the wind disturbance. Similar to experiment 1, steady-state errors were not observed implying that the proposed disturbance observer fully rejected gravity and fully compensated the wind disturbance. On comparing Figs.11 and 9, the tracking

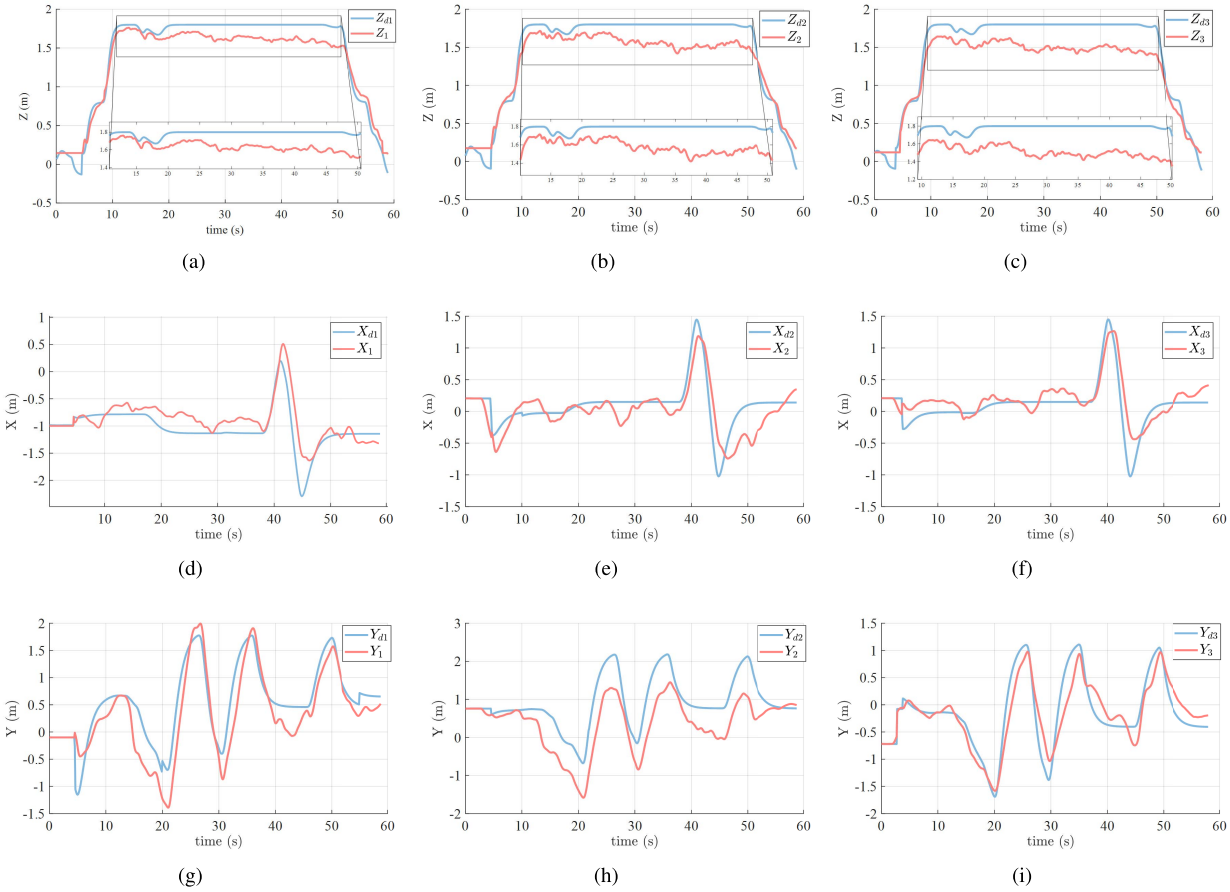

FIGURE 13. Resulting logs of each quadcopter in the experiment 2 without the force disturbance observer and torque disturbance observer. Blue lines are the target positions and red lines are the actual positions.

effectiveness of the paths do not change dramatically even under the wind disturbance. This confirms the validity of the proposed disturbance observer.

Fig. 12 shows the estimated torque and force disturbances for each quadcopter. Here, (a)–(c) show the estimated torque disturbance. No significant torque disturbance was observed for the vast majority of the flight because the hanging point of the payload was the geometric center of the quadcopter. However, in the time period of 70–90 s, because the payload suspension point was slightly off the geometric center of quadcopter due to the change in geometric formation and the increased windward surface yielded the observed torque disturbance peak for a period of time owing to the tilting of the quadcopter, and then the observed torque disturbance decreased again after the quadcopter returned to formation 1.

Fig. 12 (d)–(f) show the estimated force disturbance for each quadcopter. For quadcopter 1, the force disturbance in the horizontal plane mainly appeared along the $\vec{e}_1$ axis and that in the vertical direction was mainly caused by its own gravity and cable-suspended payload gravity. However, for quadcopters 2 and 3, horizontal force disturbances were mainly found along the $\vec{e}_2$ axis.The force disturbances in the vertical direction were also mainly caused by their own gravity and cable-suspended payload gravity. The force disturbances acting on quadcopters 2 and 3 became significantly stronger after the formation geometry changed in the period of 70 s to 90 s, which is reflected in the convexity part of the curve in (e).

To verify the effect of the force disturbance observer and torque disturbance observer on the disturbance rejection ability of the system, we conducted an experiment under the same condition as in Fig. 10 by removing the disturbance observer from the control scheme. Fig. 13 shows the target positions and actual positions of three quadcopters with cable-suspended payload under wind disturbance without force disturbance observer and torque disturbance observer. By comparing the experimental results in Fig. 11 and Fig. 13, we can see that, in Fig. 13, although the quadcopters can still track the given trajectory and maintain formation to a certain extent by relying on the robustness of the back stepping force controller and thrust direction controller, tracking errors caused by gravity exist in the Z direction due to the lack of the compensation of disturbance observer. It is also confirmed that the trajectory tracking ability in the X, Y directions is also degraded, especially for the second quadcopter, which is closest to the wind disturbance generator.

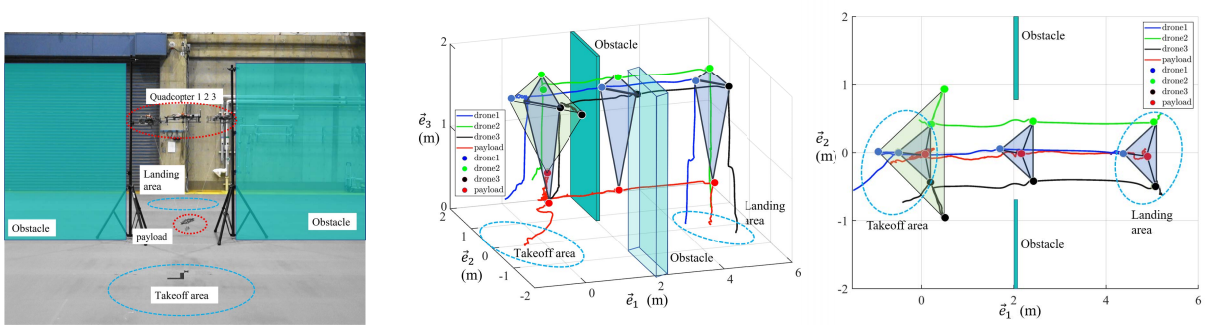

(a) (b) (c)

FIGURE 14. Experiment setup for first scenario. (a) shows a snapshot of the experiment. (b) and (c) show the trajectory of three quadcopters and a payload.

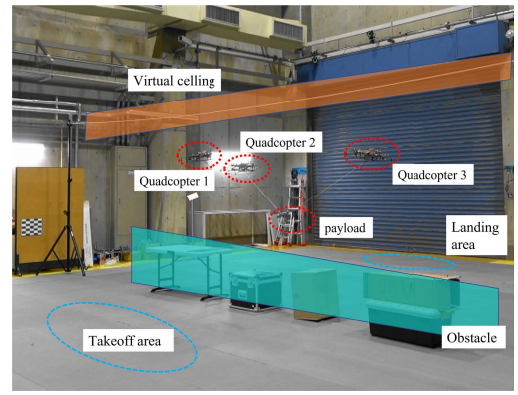

(a)

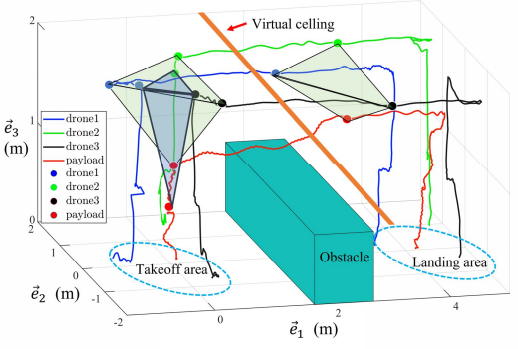

(b)

FIGURE 15. Experiment setup for second scenario. (a) shows a snapshot of the experiment. (b) shows the trajectory of three quadcopters and a payload.

D. EXPERIMENT 3: DYNAMIC FORMATION FOR FLIGHT IN CONSTRAINED ENVIRONMENT

Here, two experiments were conducted to demonstrate that dynamic formation change of three quadcopters with a cable-suspended payload can be used to avoid obstacles. Two scenarios were considered. In the first scenario, the quadcopters carried the payload through a vertical narrow slit. It was assumed that the quadcopters cannot overcome the obstacle by raising their altitude.

Fig. 14 shows the experiment for the first scenario. (a) is a snapshot of the experimental setup. Two tripods were used as virtual walls and the quadcopters tried to travel through the space between the tripods with a cable-suspended payload. The distance between the two tripods was 1.4 m. (b) and (c) show the actual trajectory of the quadcopters and payload. To travel through the vertical narrow slit, the relative formation vectors were set as $\gamma_2 = [1\ 0.6\ 0]^T$, $\gamma_3 = [1\ -0.6\ 0]^T$. From the trajectories, it is evident that the quadcopters successfully passed through the vertical narrow slit and carried the payload to the landing area.

In the second scenario, the quadcopters avoided ground obstacles and passed through a horizontal narrow slit with a ceiling. This implies that the quadcopters cannot avoid the obstacle by raising their altitude. Considering that in experiments 1 and 2, the formation geometry can be transformed in such a way that the position of the payload can be changed without changing the quadcopters' own altitude, this result suggests that changing the formation geometry is an effective way to solve the problem in this case.

Fig. 15 shows the second experimental scenario and actual trajectory of each quadcopter and payload. Fig. 15(a) shows experiment setup where a rope was used as a virtual ceiling and its height from ground was 2 m. Immediately below the rope was a wall of obstacles made up of boxes and its height was 0.8 m. For safety reasons, the quadcopters were set to maintain a flight height of 1.8 m to avoid hitting the virtual ceiling. The cable used to carry the payload was 1.2 m long; thus, without suitable formation, the payload would crash into the obstacle. Therefore, the relative formation vector was set as $\gamma_2 = [1.65\ 0.95\ 0]^T$, $\gamma_3 = [1.65\ -0.95\ 0]^T$ to ensure that the payload was as far as possible from the obstacle in the vertical direction. Fig. 15(b) shows the resulting trajectories. The results show that after take-off, the three quadcopters raised the altitude of the payload by changing the formation geometry. Moreover, during the formation geometry change, the quadcopters only moved horizontally while the altitude remained constant. Subsequently, the quadcopters

successfully carried the payload through the horizontal narrow slit between obstacle wall and virtual ceiling and reached the landing area.

VI. CONCLUSION

This study proposed a leader–follower dynamic formation approach based on virtual structures to exploit the mobility and flexibility of multi-quadcopter payload transportation systems. A force controller without any assumptions regarding the cable tension was designed to control the movement of multi-quadcopter cable-suspended payload transportation system. Further, a force direction controller was designed to ensure that the thrust of each quadcopter can track the force vector provided by the force controller. The stability of the control systems was proofed and the region of attraction was provided.

The force and torque disturbance observers were proposed to enhance the disturbance rejection ability of the quadcopters. The disturbance observers only required a control signal and a few feedback signals from sensors to estimate the internal and external disturbances. The performance of the proposed dynamic formation approach with controller and disturbance observers was validated through several indoor real flight experiments. The results showed that the proposed approach can perform effectively under heavy wind disturbance and avoid obstacles to reach the target location using formation change.

There are certain aspects that need further research to achieve better results. For example, the integrated control of the forces of all quadcopters is required to solve the mutual pulling problem between quadcopters. In addition, time-optimal and energy-optimal trajectory planning research is another necessary aspect to ensure practical use of the multi-quadcopter cable-suspended payload transportation system. Finally, outdoor flight should be investigated.

REFERENCES

[1] J. Lee, "Optimization of a modular drone delivery system," in *Proc. Annu. IEEE Int. Syst. Conf. (SysCon)*, Apr. 2017, pp. 1–8.

[2] I. Hong, M. Kuby, and A. Murray, "A deviation flow refueling location model for continuous space: A commercial drone delivery system for urban areas," in *Advances in Geocomputation*. Cham, Switzerland: Springer, 2017, pp. 125–132.

[3] Y. Mualla, A. Najjar, S. Galland, C. Nicolle, and I. H. Tchappi, "Between the megalopolis and the deep blue sky: Challenges of transport with UAVs in future smart cities," in *Proc. Int. Conf. Auto. Agents MultiAgent Syst. (AAMAS)*, 2019, pp. 1649–1653.

[4] U. A. Fiaz, M. Abdelkader, and J. S. Shamma, "An intelligent gripper design for autonomous aerial transport with passive magnetic grasping and dual-impulsive release," in *Proc. IEEE/ASME Int. Conf. Adv. Intell. Mechatronics (AIM)*, Jul. 2018, pp. 1027–1032.

[5] H. Lee, H. Kim, and H. J. Kim, "Planning and control for collision-free cooperative aerial transportation," *IEEE Trans. Autom. Sci. Eng.*, vol. 15, no. 1, pp. 189–201, Jan. 2018.

[6] R. G. Braga, R. C. da Silva, A. C. B. Ramos, and F. Mora-Camino, "UAV swarm control strategies: A case study for leak detection," in *Proc. 18th Int. Conf. Adv. Robot. (ICAR)*, Jul. 2017, pp. 173–178.

[7] D. Srivastava, R. Pakkar, A. Langrehr, and C. Yamane, "Adaptable UAV swarm autonomy and formation platform," in *Proc. IEEE Aerosp. Conf.*, Mar. 2019, pp. 1–6.

[8] S.-J. Chung, A. A. Paranjape, P. Dames, S. Shen, and V. Kumar, "A survey on aerial swarm robotics," *IEEE Trans. Robot.*, vol. 34, no. 4, pp. 837–855, Aug. 2018.

[9] G. Ganga and M. M. Dharmana, "MPC controller for trajectory tracking control of quadcopter," in *Proc. Int. Conf. Circuit, Power Comput. Technol. (ICCPCT)*, Apr. 2017, pp. 1–6.

[10] T. Lee, K. Sreenath, and V. Kumar, "Geometric control of cooperating multiple quadrotor UAVs with a suspended payload," in *Proc. 52nd IEEE Conf. Decis. Control*, Dec. 2013, pp. 5510–5515.

[11] T. Lee, "Geometric control of quadrotor UAVs transporting a cable-suspended rigid body," *IEEE Trans. Control Syst. Technol.*, vol. 26, no. 1, pp. 255–264, Jan. 2018.

[12] P. J. Cruz and R. Fierro, "Cable-suspended load lifting by a quadrotor UAV: Hybrid model, trajectory generation, and control," *Auto. Robots*, vol. 41, no. 8, pp. 1629–1643, Dec. 2017.

[13] X. Liang, Y. Fang, N. Sun, and H. Lin, "Nonlinear hierarchical control for unmanned quadrotor transportation systems," *IEEE Trans. Ind. Electron.*, vol. 65, no. 4, pp. 3395–3405, Apr. 2018.

[14] M. Jafarinasab and S. Sirouspour, "Adaptive motion control of aerial robotic manipulators based on virtual decomposition," in *Proc. IEEE/RSJ Int. Conf. Intell. Robots Syst. (IROS)*, Sep. 2015, pp. 1858–1863.

[15] K. Mohammadi, M. Jafarinasab, S. Sirouspour, and E. Dyer, "Decentralized motion control in a cabled-based multi-drone load transport system," in *Proc. IEEE/RSJ Int. Conf. Intell. Robots Syst. (IROS)*, Oct. 2018, pp. 4198–4203.

[16] K. Mohammadi, S. Sirouspour, and A. Grivani, "Control of multiple quad-copters with a cable-suspended payload subject to disturbances," *IEEE/ASME Trans. Mechatronics*, vol. 25, no. 4, pp. 1709–1718, Aug. 2020.

[17] S. Waslander and C. Wang, "Wind disturbance estimation and rejection for quadrotor position control," in *Proc. AIAA Infotech@ Aerosp. Conf.*, 2009, pp. 1935–1948.

[18] P. V. Tran, F. Santoso, M. A. Garratt, and I. R. Petersen, "Adaptive second-order strictly negative imaginary controllers based on the interval type-2 fuzzy self-tuning systems for a hovering quadrotor with uncertainties," *IEEE/ASME Trans. Mechatronics*, vol. 25, no. 1, pp. 11–20, Feb. 2020.

[19] H. Yang, L. Cheng, Y. Xia, and Y. Yuan, "Active disturbance rejection attitude control for a dual closed-loop quadrotor under gust wind," *IEEE Trans. Control Syst. Technol.*, vol. 26, no. 4, pp. 1400–1405, Jul. 2018.

[20] H. Rios, R. Falcon, O. A. Gonzalez, and A. Dzul, "Continuous sliding-mode control strategies for quadrotor robust tracking: Real-time application," *IEEE Trans. Ind. Electron.*, vol. 66, no. 2, pp. 1264–1272, Feb. 2019.

[21] F. Kendoul, "Nonlinear hierarchical flight controller for unmanned rotorcraft: Design, stability, and experiments," *J. Guid., Control, Dyn.*, vol. 32, no. 6, pp. 1954–1958, Nov. 2009.

[22] Z. Gao, "Scaling and bandwidth-parameterization based controller tuning," in *Proc. Amer. Control Conf.*, Jun. 2003, pp. 4989–4996.

XIAO HAN received the M.S. degree from the Graduate School of Systems and Information Engineering, University of Tsukuba, Japan, in 2021. He is currently pursuing the Ph.D. degree with the University of Tsukuba. His research interests include controller designing and disturbance rejection of unmanned aerial vehicle, development of control systems, and path planning for multiple robotic cooperation systems.

RYO MIYAZAKI (Member, IEEE) received the M.E. and Ph.D. degrees in mechanical engineering from Ritsumeikan University, Japan, in 2019 and 2022, respectively. He has been a Postdoctoral Fellow at the Industrial Cyber-Physical Systems Research Center (ICPS), National Institute of Advanced Industrial Science and Technology (AIST), since April 2022. His research interests include development of aerial manipulators, control systems with sensor fusion and onboard vision system for unmanned aerial vehicle (UAV), path planning for multi UAVs, and teleoperation system with VR. He is a member of RSJ. His research was chosen as one of the finalists for IROS 2018 Best Paper Award.

TIANHUA GAO received the B.S. degree in automation from the Shanghai University of Engineering Science, Shanghai, China, in 2020. He is currently pursuing the M.S. degree with the Graduate School of Systems and Information Engineering, University of Tsukuba, Tsukuba, Japan. He is also working as a Research Assistant with the Field Robotics Research Team, Industrial Cyber-Physical Systems Research Center, National Institute of Advanced Industrial Science and Technology (AIST), Tsukuba. He is also with the Graduate School of Systems and Information Engineering, University of Tsukuba, and the Industrial Cyber-Physical Systems Research Center, AIST. His research interests include multi-UAVs control and autonomous UAV recovery systems.

KOHJI TOMITA (Member, IEEE) received the B.E., M.E., and Ph.D. degrees from the University of Tsukuba, in 1988, 1990, and 1997, respectively. He joined the Mechanical Engineering Laboratory, National Institute of Advanced Industrial Science and Technology (AIST), MITI, in 1990, and has been conducting research as a Senior Research Scientist at the AIST, since 2001. He was a Visiting Researcher at the Dartmouth College, from 2000 to 2001. His research interests include modular robots, distributed software systems, graph automata, and smart mobility systems.

AKIYA KAMIMURA (Member, IEEE) received the M.E. and Ph.D. degrees from the Graduate School of Engineering, The University of Tokyo, in 1997 and 2000, respectively. He joined the Mechanical Engineering Laboratory, National Institute of Advanced Industrial Science and Technology (AIST), MITI, in 2000, and has been conducting research at the AIST, since 2001. From March 2009 to March 2010, he was a Visiting Researcher at the Information Sciences Institute, University of Southern California, USA. Since 2017, he has been an Associate Professor with the Partner Graduate School of Master and Doctoral Programs in Intelligent and Mechanical Systems, University of Tsukuba, and has been a Professor, since 2021. He has authored more than 70 articles, and has acquired 17 patents in Japan, EPO, USA, Germany, and U.K. His research interests include modular robotics, field robotics, infrastructure inspection robots, and the IoT communication systems. He received the Best Paper Award at the international conferences, in 2002, 2003, 2006, and 2018.